PHOTONIC SENSORS / Vol. 7, No. 3, 2017: 217–225

A Study on Refractive Index Sensors Based on Optical Micro-Ring Resonators

Georgios N. TSIGARIDAS*

Department of Physics, School of Applied Mathematical and Physical Sciences, National Technical University of Athens, Zografou Campus, GR-15780 Zografou, Athens, Greece

*Corresponding author: Georgios N. TSIGARIDAS E-mail: gtsig@mail.ntua.gr

Abstract: In this work, the behavior of refractive index sensors based on optical micro-ring resonators is studied in detail. Using a result of waveguide perturbation theory in combination with numerical simulations, the optimum design parameters of the system, maximizing the sensitivity of the sensor, are determined. It is found that, when optimally designed, the sensor can detect relative refractive index changes of the order of $\Delta n/n \approx 3\times10^{-4}$, assuming that the experimental setup can detect relative wavelength shifts of the order of $\Delta\lambda/\lambda \approx 3\times10^{-5}$. The behavior of the system as bio-sensor has also been examined. It is found that, when optimally designed, the system can detect refractive index changes of the order of $\Delta n \approx 10^{-3}$ for a layer thickness of t=10 nm, and changes in the layer thickness of the order of $\Delta t \approx 0.24$ nm, for a refractive index change of Δn=0.05.

Keywords: Optical micro-ring resonators; refractive index sensors; bio-sensors; nano-photonic sensors

Citation: Georgios N. TSIGARIDAS, "A Study on Refractive Index Sensors Based on Optical Micro-Ring Resonators," *Photonic Sensors*, 2017, 7(3): 217–225.

1. Introduction

Optical ring resonators are interesting optical devices with a plethora of applications especially in optical switching [1–4], routing [4–7], and sensing [8–10]. An optical ring resonator usually consists of a straight waveguide coupled to a circular one, as shown in Fig. 1(a), or two straight waveguides coupled through a circular one, as shown in Fig. 1(b).

In the first case the transmittance is given by the formula [11]

$$T_n = \frac{a^2 + r^2 - 2ar\cos\varphi}{1 + r^2a^2 - 2ar\cos\varphi} \tag{1}$$

where r is the self-coupling coefficient of light between the straight and circular waveguides, and a is a loss parameter related to the power attenuation coefficient α through the equation $a^2=\exp(-\alpha L)$, with L being the length of the circular waveguide. Here, φ is the single-pass phase shift, defined as

$$\varphi = \beta L = \frac{2\pi n_{\text{eff}}}{\lambda_0} L \tag{2}$$

where β is the propagation constan, n_{eff} the effective refractive index of the propagating mode in the circular waveguide, and λ_0 the free space wavelength. Setting $\cos\varphi \to y$, (1) takes the form:

$$T_n = \frac{a^2 + r^2 - 2ary}{1 + r^2a^2 - 2ary}. \tag{3}$$

The derivative of T_n with respect to y is as follows:

$$\frac{dT_n}{dy} = -\frac{2a\left(-1+a^2\right)r\left(-1+r^2\right)}{\left(1+a^2r^2-2ary\right)^2}. \tag{4}$$

It is obvious that $dT_n/dy \le 0$ since both a and r

Received: 23 March 2017 / Revised: 28 May 2017

DOI: 10.1007/s13320-017-0418-0
Article type: Regular

are less than or equal to unity. Thus, the transmittance is minimized for y=1, which implies that the condition for minimum transmittance, as far as the phase shift is concerned, is

$$\cos\varphi = 1 \quad \text{or} \quad \varphi = 2m\pi \tag{5}$$

where m is an integer. From (2) and (5), it follows that the values of the wavelength minimizing the transmittance (resonant wavelengths) are given by the formula

$$\lambda_{0,\text{res}} = \frac{L}{m} n_{\text{eff}} = \frac{2\pi R}{m} n_{\text{eff}} \tag{6}$$

where R is the radius of the circular waveguide. In this case the transmittance takes the form

$$T_{n,\text{res}} = \left(\frac{a-r}{1-ar} \right)^2 \tag{7}$$

which implies that for $a = r$, critical coupling, the transmittance is zero.

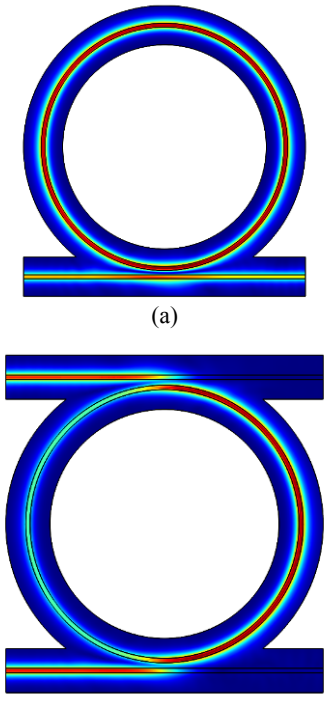

(a)

(b)

Fig. 1 Two basic configurations of an optical micro-ring resonator: (a) a linear waveguide is coupled to a circular one, and (b) two linear waveguides are coupled to each other through a circular one.

As far as the arrangement shown in Fig. 1(b) is concerned, the transmittance through the lower and upper waveguides are given by the formulae

$$T_p = \frac{r_1^2 + a^2 r_2^2 - 2ar_1 r_2 y}{1 + a^2 r_1^2 r_2^2 - 2ar_1 r_2 y} \tag{8a}$$

and

$$T_d = \frac{a\left(1-r_1^2\right)\left(1-r_2^2\right)}{1 + a^2 r_1^2 r_2^2 - 2ar_1 r_2 y} \tag{8b}$$

respectively. Here r_1 and r_2 are the coupling coefficients between the lower-circular and upper-circular waveguides respectively and $y = \cos\varphi$. Following a similar analysis it can be shown that the condition for the minimum transmittance through the lower waveguide, and simultaneously the maximum transmittance through the upper waveguide, is described again by (6). In this case (8a) and (8b) take the form

$$T_{p,\text{res}} = \left(\frac{r_1 - ar_2}{1 - ar_1 r_2} \right)^2 \tag{9a}$$

and

$$T_{d,\text{res}} = \frac{a\left(1-r_1^2\right)\left(1-r_2^2\right)}{\left(1-ar_1 r_2\right)^2}. \tag{9b}$$

Equation (9a) implies that for $r_1 = ar_2$, T_p=0. In this case the transmittance through the upper waveguide takes the form

$$T_{d,\text{res}}\big|_{r_1 = ar_2} = \frac{a\left(r_2^2 - 1\right)}{a^2 r_2^2 - 1}. \tag{10}$$

It is obvious that for $a = 1$, $T_d = 1$. Thus, in the case of a symmetrical optical ring resonator, shown in Fig. 1(b), the light is perfectly coupled to the upper waveguide, when the wavelength is given by (6), the loss parameter is equal to unity $(a = 1)$, and the coupling coefficients are equal to each other $(r_1 = r_2)$.

As far as the use of micro-ring resonators as refractive index sensors is concerned, the most important result of the above analysis is that, in both configurations, the resonant wavelength is given by (6), which practically implies that it is proportional to the effective refractive index of the propagating mode in the circular waveguide. However, the value of n_{eff} depends on the refractive index of the environment. Therefore, the system can function as

a refractive index sensor. In more detail, supposing that the effective refractive index changes by Δn_{eff} due to a change in the refractive index of the environment by Δn, (6) takes the form

$$\lambda_{0,\text{res}} + \Delta\lambda_{0,\text{res}} = \frac{2\pi R}{m}\left(n_{\text{eff}} + \Delta n_{\text{eff}}\right) \tag{11}$$

where $\Delta\lambda_{0,\text{res}}$ is the corresponding change in the resonant wavelength. Dividing (11) and (6) by parts follows that:

$$\frac{n_{\text{eff}} + \Delta n_{\text{eff}}}{n_{\text{eff}}} = \frac{\lambda_{0,\text{res}} + \Delta\lambda_{0,\text{res}}}{\lambda_{0,\text{res}}} \quad \text{or} \quad \frac{\Delta n_{\text{eff}}}{n_{\text{eff}}} = \frac{\Delta\lambda_{0,\text{res}}}{\lambda_{0,\text{res}}}. \tag{12}$$

Consequently, the relative change in the resonant wavelength is equal to the relative change in the effective refractive index.

According to the above analysis, the most important parameter regarding the performance of an optical ring resonator when used as a refractive index sensor is the dependence of the effective refractive index of the propagating mode on the refractive index of the environment. Mathematically, this is described by the quantity as

$$S = \frac{1}{n_{\text{eff}}}\frac{dn_{\text{eff}}}{dn} \quad \text{or} \quad S = \frac{1}{n_{\text{eff}}}\frac{\Delta n_{\text{eff}}}{\Delta n} \tag{13}$$

where in the second form of (13), it is supposed that the refractive index change of the environment is sufficiently small, so that the dependence of Δn_{eff} on Δn is linear. Using the parameter S, (12) takes the form:

$$\frac{\Delta\lambda_{0,\text{res}}}{\lambda_{0,\text{res}}} = S\Delta n. \tag{14}$$

From (14), it is obvious that S can be regarded as a measure of the sensitivity of the system when used as a refractive index sensor. In practice, the parameter S can be numerically calculated quite easily as described in the following section.

2. Numerical analysis

The profile and effective refractive indexes of the propagating modes in the circular waveguide are calculated using the finite element analysis [12]. The simulations were assisted by the Comsol Multiphysics software package. The analysis is made on a two dimensional cross-section of the waveguide, assuming that its profile and properties remain constant throughout its length. Firstly, the electromagnetic field is written in the form

$$\begin{aligned} E(x,y,z) &= A(x,y)\exp(-\alpha_0 z)\exp(\mathrm{i}\beta z) \\ &= A(x,y)\exp(-\gamma z) \end{aligned} \tag{15a}$$

$$\begin{aligned} H(x,y,z) &= B(x,y)\exp(-\alpha_0 z)\exp(\mathrm{i}\beta z) \\ &= B(x,y)\exp(-\gamma z) \end{aligned} \tag{15b}$$

where $E(x,y,z)$ and $H(x,y,z)$ are the electric and magnetic field components of the propagating wave, respectively. The two-dimensional functions $A(x,y)$ and $B(x,y)$ describe the mode profile, assuming that the electromagnetic wave is propagating in the $+z$ direction. Here α_0 is the linear loss coefficient and β is the propagation constant, related to the effective refractive index through the formula as

$$\beta = k_0 n_{\text{eff}} \tag{16}$$

where $k_0 = 2\pi/\lambda_0$ is the free space wavenumber. The parameter γ corresponds to the generalized propagation constant, defined as $\gamma = \alpha_0 - \mathrm{i}\beta$.

Writing the Maxwell equations in matrix form and eliminating the longitudinal field components, an eigenvalue problem of the form

$$\mathbf{\Omega}^2\begin{bmatrix}\mathbf{A}_x\\ \mathbf{A}_y\end{bmatrix} = \left(\frac{\gamma}{k_0}\right)^2\begin{bmatrix}\mathbf{A}_x\\ \mathbf{A}_y\end{bmatrix} \tag{17}$$

is obtained, where

$$\mathbf{\Omega}^2 = \begin{bmatrix} \mathbf{D}^e_{x'}\varepsilon_{zz}^{-1}\mathbf{D}^h_{y'} & -\left(\mathbf{D}^e_{x'}\varepsilon_{zz}^{-1}\mathbf{D}^h_{x'} + \mu_{yy}\right) \\ \mathbf{D}^e_{y'}\varepsilon_{zz}^{-1}\mathbf{D}^h_{y'} + \mu_{xx} & \mathbf{D}^e_{y'}\varepsilon_{zz}^{-1}\mathbf{D}^h_{x'} \end{bmatrix}\times \begin{bmatrix} \mathbf{D}^h_{x'}\mu_{zz}^{-1}\mathbf{D}^e_{y'} & -\left(\mathbf{D}^h_{x'}\mu_{zz}^{-1}\mathbf{D}^e_{x'} + \varepsilon_{yy}\right) \\ \mathbf{D}^h_{y'}\mu_{zz}^{-1}\mathbf{D}^e_{y'} + \varepsilon_{xx} & \mathbf{D}^h_{y'}\mu_{zz}^{-1}\mathbf{D}^e_{x'} \end{bmatrix}. \tag{18}$$

where $\mathbf{D}^e_{x'(y')}$ and $\mathbf{D}^h_{x'(y')}$ are matrix differential operators with respect to $x'(y')$ for the electric and magnetic field respectively, and ε_{xx}, ε_{yy}, ε_{zz}, μ_{xx}, μ_{yy}, and μ_{zz} are matrices containing the diagonal elements of the relative permittivity and permeability tensors at each position. The vector matrix $\begin{bmatrix}\mathbf{A}_x\\ \mathbf{A}_y\end{bmatrix}$ corresponds to the transverse

distribution of the electric field, $A(x, y)$, with $\mathbf{A}_x$ and $\mathbf{A}_y$ containing in single column format the x and y components of the electric field at each position. The coordinates (x', y', z') are related to (x, y, z) through the transformation $(x' \to k_0 x, y' \to k_0 y, z' \to k_0 z)$.

Thus, solving (17) for the eigenvalues $\lambda = (\gamma / k_0)^2$ and the eigenvectors $\begin{bmatrix} \mathbf{A}_x \\ \mathbf{A}_y \end{bmatrix}$, the generalized propagation constant and consequently the effective refractive index as well as the transverse electric field distribution (profile) for each mode are obtained.

It should be noted that in most applications of practical interest, the single mode operation is preferable, because the existence of more than one propagating modes would complicate the behavior of the system. For example, in the case of multi-mode operation, (6) implies that more than one resonant wavelengths exist for each configuration, which would result in multiple dips (or peaks, if measured through the upper waveguide) in the transmittance spectrum, complicating both the theoretical and experimental analysis of the system. Therefore, in the simulations, special care is taken in order to ensure single mode operation.

3. Simulations, results, and discussion regarding design optimization

According to a result of waveguide perturbation theory [13], the change in the effective refractive index of the propagating mode due to a refractive index change in some part of the waveguide is proportional to the fraction of the mode power in this specific part of the waveguide, defined as

$$\eta_p = \frac{\iint_{S_p} |A(x,y)|^2 \, dxdy}{\iint_{S_{\text{tot}}} |A(x,y)|^2 \, dxdy} \tag{18}$$

where S_p is the area where the refractive index has changed and S_{tot} is the total area of the waveguide. Further, according to (13), the sensitivity S is proportional to Δn_{eff} and consequently it will also be proportional to η_p. This practically means that the sensitivity increases as the overlapping of the propagating mode with its environment becomes more extensive.

Therefore, in the simulations the core of the waveguide is considered to be in direct contact with the environment. Further, the core dimensions are chosen to be small, close to the limit of waveguiding, in order to increase the mode spreading and maximize the parameter η_p. The cross section of the core of the waveguide is considered to be rectangular, as shown in Fig. 2, where the mode profile is also depicted, for two different heights of the waveguide core. The material of the core is chosen to be silicon nitride (SiN), which has the advantage that its refractive index is relatively insensitive to temperature fluctuations [14, 15]. It is supposed that the core is developed on a layer of SiO_2, as usually happens in practice. The environment is chosen to be water, which is the most common solvent, and it is also suitable for biological applications. Thus, the simulation model consists of a vertical column of SiN with small dimensions (the core of the waveguide) developed on a horizontal layer of SiO_2, while all the system is submersed in water. The free space wavelength is supposed to be λ_0=1550 nm, which is a common wavelength emitted by fiber lasers, and further corresponds to the minimum of the fiber losses [16].

The refractive indices of the materials used in the simulations at the aforementioned wavelength are [17] $n_{\text{SiN}} = 2.463$, $n_{\text{SiO}_2} = 1.443$, and $n_{\text{water}} = 1.318$ for the silicon nitride, silicon dioxide, and water, respectively. The dimensions of the waveguide core are chosen to be $h = \lambda_{\text{env}}$ and $w = \lambda_{\text{env}} / 4$, where h is the height and w the width of the waveguide, while $\lambda_{\text{env}} = \lambda_0 / n_{\text{env}}$ is the wavelength in the environment of the sensor, water in our case. This choice for the dimensions of the waveguide core ensures single mode operation and sufficient mode spreading. In order to optimize

further the design of the refractive index sensor the parameter η_p is calculated as a function of the core width w with the height fixed to $h=\lambda_{\text{env}}$. The results are shown in Fig. 3, where it is clear that the maximum value of η_p is obtained for $w=0.175\ \lambda_{\text{env}}$.

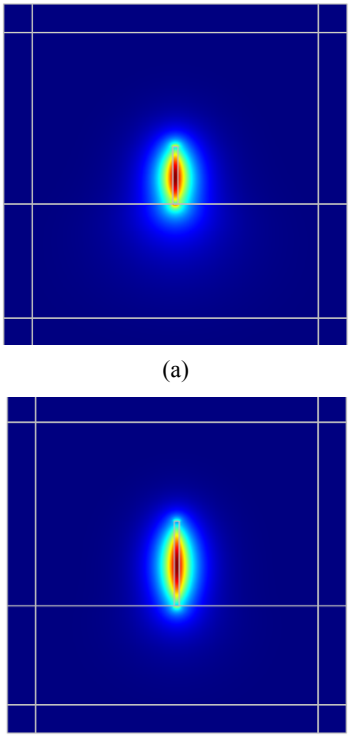

(a)

(b)

Fig. 2 Profile of the fundamental mode in a single core waveguide in the case of (a) $h=\lambda_{\text{env}}$ and (b) $h=3\lambda_{\text{env}}/2$. In both cases the waveguide width is $w=0.175\lambda_{\text{env}}$.

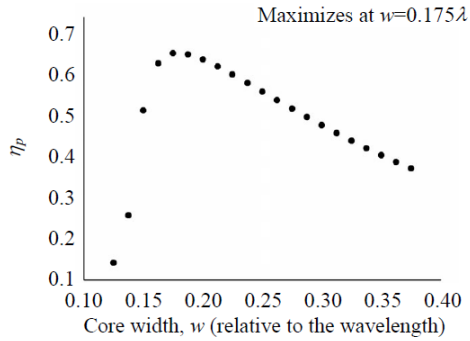

Fig. 3 Values of the parameter η_p as function of the core width w in the case of $h=\lambda_{\text{env}}$.

In order to optimize the height of the waveguide, the parameter η_p is calculated as the function of the waveguide height, with the width fixed to $w=0.175\lambda_{\text{env}}$. The results are shown in Fig. 4. It is clear that the value of η_p does not change much for $h\geq\lambda_{\text{env}}$. Further, for $h>3\lambda_{\text{env}}/2$, the multimode behavior is exhibited, which is not desirable for practical applications, as explained in the previous section. Thus, the optimum width of the waveguide core is $w_{\text{opt}}=0.175\ \lambda_{\text{env}}$ while the optimum height lies in the region $\lambda_{\text{env}}\leq h_{\text{opt}}\leq 3\lambda_{\text{env}}/2$.

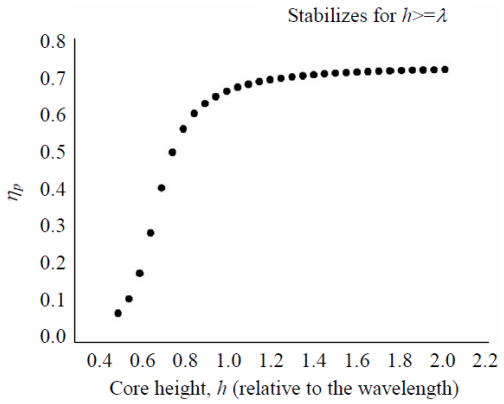

Fig. 4 Values of the parameter η_p as function of the core height h in the case of $w=0.175\lambda_{\text{env}}$.

A double core configuration has also been studied, as shown in Fig. 5, where the mode profile is depicted. In this case, the dimensions of each core are chosen to be $w=0.175\ \lambda_{\text{env}}$ and $h=\lambda_{\text{env}}$. Higher values of h have not been considered because the system exhibits multi-mode operation. In order to find the optimum distance between the fiber cores, the parameter η_p has been calculated as function of the core separation d. The results are shown in Fig. 6.

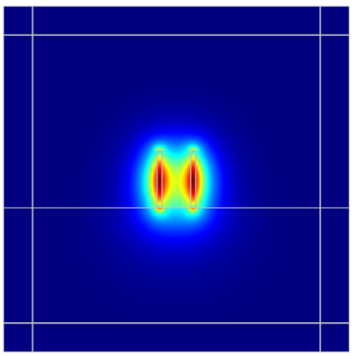

Fig. 5 Profile of the fundamental mode in a dual core waveguide in the case of $h=\lambda_{\text{env}}$, $w=0.175\lambda_{\text{env}}$, and $d=\lambda_{\text{env}}/2$.

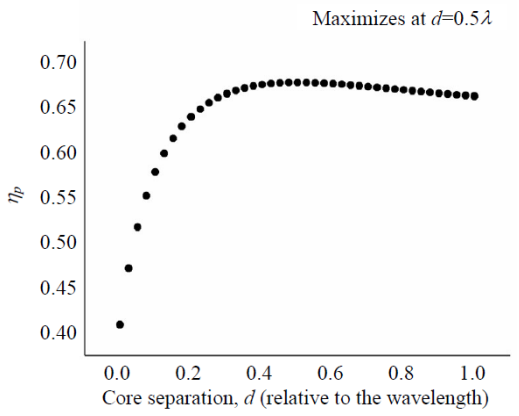

Fig. 6 Values of the parameter η_p as function of the core separation d in the case of $w=0.175\lambda_{env}$ and $h=\lambda_{env}$.

It is clear that η_p is maximized for $d=\lambda_{env}/2$. Thus, the optimum conditions for a dual core design are $w_{opt}=0.175\ \lambda_{env}$, $h_{opt}=\lambda_{env}$, and $d_{opt}=\lambda_{env}/2$. It should be noted that although these optimal values refer to an incident wavelength of 1 550 nm, they can be used as guidelines for other wavelengths. This is due to the fact that the Maxwell equations are invariant under scale transformations and consequently the behavior of the system does not change if its dimensions are scaled according to the wavelength ratio. For example, if the wavelength is multiplied by a factor x and all the dimensions of the waveguide are multiplied by the same factor, then its behavior will remain unchanged. Of course, in practice this cannot be achieved because the optical properties of the materials change due to dispersion. However, in any case, these values can be used as good starting points for the design optimization. Next, the sensitivity is calculated for the three optimal configurations, specifically $w=0.175\ \lambda_{env}$, $h=\lambda_{env}$, single core, $w=0.175\ \lambda_{env}$, $h=3\lambda_{env}/2$, single core, and $w=0.175\ \lambda_{env}$, $h=\lambda_{env}$, $d=\lambda_{env}/2$, dual core. The results are shown in Table 1.

Table 1: Basic characteristics of the three optimal designs described above.

No. of cores	w/λ_{env}	h/λ_{env}	d/λ_{env}	n_{eff}	dn_{eff}/dn	S
1	0.175	1	-	1.46951	0.317	0.216
1	0.175	1.5	-	1.50435	0.330	0.219
2	0.175	1	0.5	1.50773	0.365	0.242

For these values of the sensitivity, (14) implies that the relative change in the resonant wavelength is $\Delta\lambda_{0,res}/\lambda_{0,res}=0.216\Delta n$ for a single core design $(h=\lambda_{env})$ and further increases by a factor of 1.014 in the case of $h=3\lambda_{env}/2$ and 1.120 for a dual core configuration. This practically means that if the experimental setup is able to resolve a wavelength shift of the order of $\Delta\lambda/\lambda\approx 3\times10^{-5}$, which can be easily achieved by modern high-end optical spectrum analyzers, then the system can detect a refractive index change of $\Delta n_{min}\approx 1.4\times10^{-4}$ for a single core configuration $(h=\lambda_{env})$, which is further reduced by a factor of 1.014 in the case of $h=3\lambda_{env}/2$ and 1.120 in the case of a dual core design.

It should be noted that the gain in the sensitivity for a dual core design is not that significant in order to justify the complexity of the design and the manufacturing challenges that entails. Therefore, it is suggested that in most practical situations, the design of choice would be a single core waveguide with dimensions $w=0.175\ \lambda_{env}$ and $\lambda_{env}\le h\le 3\lambda_{env}/2$. Furthermore, as it will be shown in the following section, the choice of $w=0.175\ \lambda_{env}$ and $h=3\lambda_{env}/2$ for the core dimensions provides better sensitivity than the dual core design as far as the behavior of the system as biosensor is considered.

4. Study of the bio-sensing properties of the system

In recent years, the use of photonic nano-sensors as bio-sensors is a hot topic of research, with a plethora of designs and applications [18–23]. Therefore, in the following, the behavior of the system described in the previous section as biosensor is considered. For this purpose, a thin layer of biomaterial is supposed to be attached on the surface of the waveguide core. The dependence of the parameter η_p, namely the fraction of the mode power propagating within the layer, as function of the layer thickness, is shown in Fig. 7. It is assumed

that the refractive index within the bio-layer increases by Δn=0.01 compared to the environment, although the parameter η_p is not very sensitive to the refractrive index of the biolayer.

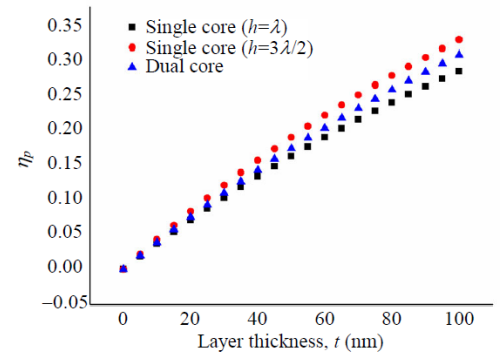

(a)

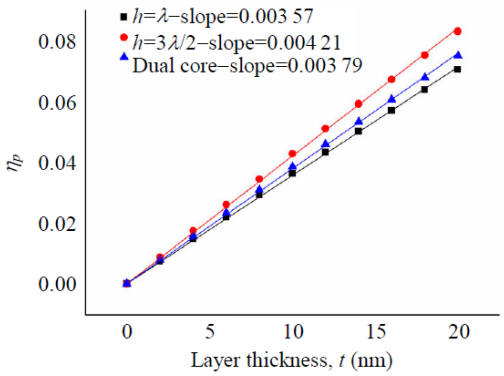

(b)

Fig. 7 Values of the parameter η_p as function of the layer thickness t for a range of (a) 100 nm and (b) 20 nm (zooming).

It is clear that η_p and consequently the sensitivity increase linearly for small values of the layer thickness but exhibit a trend for saturation as t increases beyond ~40 nm. It should also be noted that in this case the sensitivity of the single core waveguide with height h=3λ_{env}/2 is greater than that of the dual core one. In order to study the sensing ability of the system as the refractive index of the bio-layer varies, the relative change in the effective refractive index has been calculated as function of the refractive index difference of the layer material. Two values of the layer thickness are considered, namely t=10 nm and t=20 nm. The results are shown in Fig. 8.

It is clear that the dependence is linear, and further the single core waveguide with height $h = 3\lambda_{env}/2$ exhibits the highest sensitivity, with a slope of 0.026 in the case of t=10 nm and 0.050 when the layer thickness doubles. This practically means that if the experimental setup can resolve a relative change in the resonant wavelength of the order of 3×10^{-5}, then the system can sense refractive index changes within the bio-layer of the order of $\Delta n_{min} \approx 1.15\times10^{-3}$ for a layer thickness of 10 nm, which is reduced by a factor of two when the layer thickness doubles. Consequently, the system is able to detect very subtle changes in the composition or in the environment of the bio-layer. Finally, the sensing ability of the system regarding the thickness of the bio-layer has been examined. For this purpose, the values of the relative change in the effective refractive index have been calculated as function of the layer thickness, supposing that the refractive index change within the layer is $\Delta n = 0.01$ and $\Delta n = 0.05$. The results are shown in Fig. 9.

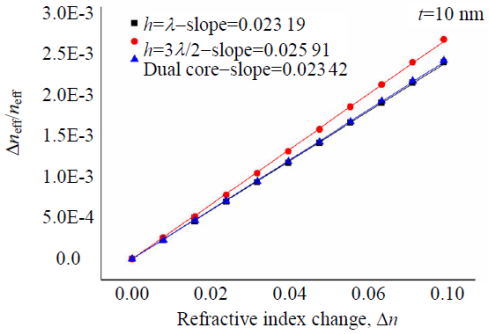

(a)

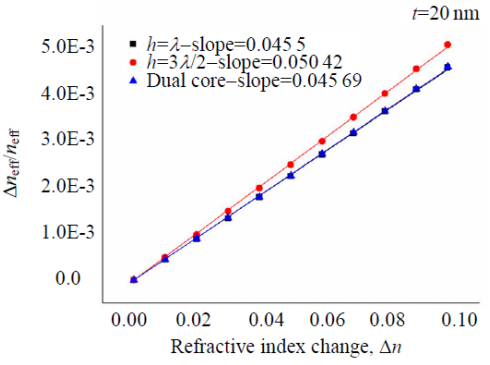

(b)

Fig. 8 Relative changes in the effective refractive index, and consequently in the resonant wavelength, as function of the refractive index change Δn in the bio-layer, when its thickness is (a) t=10 nm and (b) t=20 nm.

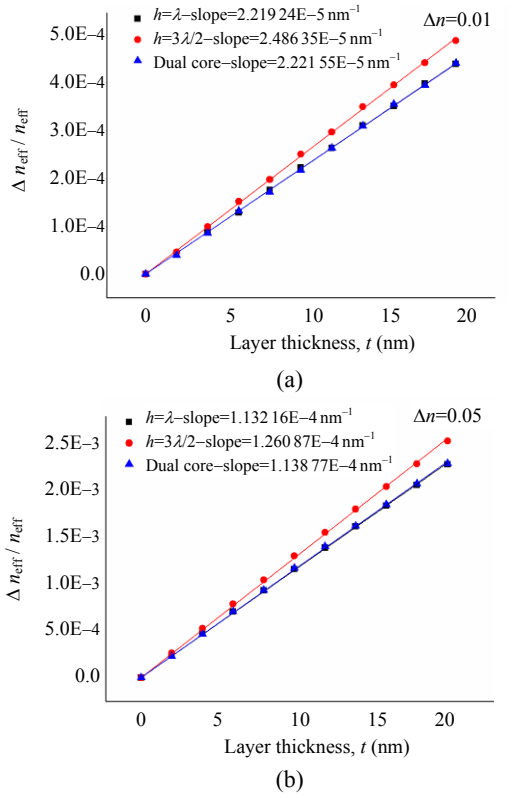

Fig. 9 Relative change in the effective refractive index, and consequently in the resonant wavelength, as function of the thickness t of the bio-layer, when the change in its refractive index is (a) $\Delta n = 0.01$ and (b) $\Delta n = 0.05$.

It is clear that the dependence is again linear, and the highest sensitivity is exhibited by the $h = 3\lambda_{env}/2$ single core waveguide. Indeed, the slope in this case is $2.49\times10^{-5}\,\mathrm{nm}^{-1}$ for $\Delta n = 0.01$ and increases to $1.26\times10^{-4}\,\mathrm{nm}^{-1}$ in the case of $\Delta n = 0.05$. Consequently, supposing that the minimum relative wavelength shift that can be measured is 3×10^{-5}, the minimum change in the layer thickness that can be detected is $\Delta t_{\min} \approx 1.2$ nm in the case of $\Delta n = 0.01$, which is further reduced to $\Delta t_{\min} \approx 0.24$ nm for $\Delta n = 0.05$. This impressive result leads to the conclusion that the system can detect even the slightest changes in the configuration of the biomolecules.

5. Conclusions

In this work the behavior of optical micro-ring resonators when functioning as refractive index sensors has been studied in detail. Detailed guidelines for maximizing the sensitivity of the sensors are provided. It is found that, when optimally designed, the system can detect relative refractive index changes of the order of $\Delta n/n \approx 10^{-4}$, assuming that the experimental setup is able to resolve relative wavelength shifts of the order of $\Delta\lambda/\lambda \approx 3\times10^{-5}$. The performance of the systems as bio-sensor has also been examined. It is found that, when optimally designed, the system can detect refractive index changes of the order of $\Delta n \approx 10^{-3}$ for a layer thickness of t=10 nm, and changes in the layer thickness of the order of $\Delta t \approx 0.24$ nm, for a refractive index change of $\Delta n \approx 0.05$.

References

[1] R. Q. Ji, L. Yang, L. Zhang, Y. H. Tian, J. F. Ding, H. T. Chen, *et al.*, "Microring-resonator-based four-port optical router for photonic networks-on-chip," *Optics Express*, 2011, 19(20): 18945–18955.

[2] R. Q. Ji, J. Xu, and L. Yang, "Five-port optical router based on microring switches for photonic networks-on-chip," *IEEE Photonics Technology Letters*, 2013, 25(5): 492–495.

[3] T. Hu, H. Shao, L. Z. Yang, C. Xu, M. Yang, H. Yu, *et al.*, "Four-port silicon multi-wavelength optical router for photonic networks-on-chip," *IEEE Photonics Technology Letters*, 2013, 25(23): 2281–2284.

[4] S. J. Emelett and R. Soref, "Design and simulation of silicon microring optical routing switches," *Journal of Lightwave Technology*, 2005, 23(4): 1800–1807.

[5] Q. Xu and M. Lipson, "All-optical logic based on silicon micro-ring resonators," *Optics Express*, 2007, 15(3): 924–929.

[6] V. Van, T. A. Ibrahim, K. Ritter, P. P. Absil, F. G. Johnson, R. Grover, *et al.*, "All-optical nonlinear switching in GaAs-AlGaAs microring resonators," *IEEE Photonics Technology Letters*, 2002, 14(1): 74–76.

[7] J. N. Xia, "Microring-resonator-based switch

architectures for optical networks," Ph.D. dissertation, Politecnico di Torino, Turin MA, 2014.
[8] I. M. White and X. Fan, "On the performance quantification of resonant refractive index sensors," *Optics Express*, 2008, 16(2): 1020–1028.
[9] M. Gabalis, D. Urbonas, and R. Petruskevicius, "A perforated microring resonator for optical sensing applications," *Journal of Optic*s, 2014, 16(10): 105003.
[10] A. Yalcin, K. C. Popat, J. C. Aldridge, T. A. Desai, J. Hryniewicz, N. Chbouki, *et al.*, "Optical sensing of biomolecules using microring resonators," *IEEE Journal of Selected Topics in Quantum Electronics*, 2006, 12(1): 148–155.
[11] W. Bogaerts, P. D. Heyn, T. V. Vaerenbergh, K. D. Vos, S. K. Selvaraja, T. Claes, *et al.*, "Silicon microring resonators," *Laser & Photonics Reviews*, 2015, 6(1): 47–73.
[12] J. M. Jin, *The finite element method in electromagnetics*. Piscataway, U.S.: Wiley, 2014.
[13] A. W. Snyder and J. D. Love, *Optical waveguide theory*. New York, U.S.: Springer US, 1983, pp. 1–37.
[14] K. B. Gylfason, C. F. Carlborg, A. Kazmierczak, F. Dortu, H. Sohlstom, L. Vivien, *et al.*, "On-chip temperature compensation in an integrated slot-waveguide ring resonator refractive index sensor array," *Optics Express*, 2010, 18(4): 3226–3237.
[15] V. Raghunathan, W. N. Ye, J. J. Hu, T. Izuhara, J. Michel, and L. Kimerling, "Athermal operation of silicon waveguides: spectral, second order and footprint dependencies," *Optics Express*, 2010, 18(17): 17631–17639.
[16] G. P. Agrawal, *Nonlinear Fiber Optics*, Pittsburgh: Academic Press, 2001, pp: 1–61.
[17] Optical constants for a variety of materials. Available online: http://refractiveindex.info/.
[18] M. Consales, M. Pisco, and A. Cusano, "Lab-on-fiber technology: a new avenue for optical nanosensors," *Photonic Sensors*, 2012, 2(4): 289–315.
[19] S. Olyaee, S. Najafgholinezhad, and H. Alipour-Banaei, "Four-channel label-free photonic crystal biosensor using nanocavity resonators," *Photonic Sensors*, 2013, 3(3): 231–236.
[20] M. Nejadebrahimy, L. Halimi, and H. Alipour-Banaei, "Design and simulation of ultrasensitive nano-biosensor based on OFPC," *Photonic Sensors*, 2015, 5(1): 43–19.
[21] S. Robinson and N. Dhanlaksmi, "Photonic crystal based biosensor for the detection of glucose concentration in urine," *Photonic Sensors*, 2017, 7(1): 11–19.
[22] X. N. Han, X. Y. Han, Y. H. Shao, Z. L. Wu, Y. X. Liang, J. Teng, *et al.*, "Polymer integrated waveguide optical biosensor by using spectral splitting effect," *Photonic Sensors*, 2017, 7(2): 131–139.
[23] H. Heng and R. Wang, "Electromagnetic resonant properties of metal-dielectric-metal (MDM) cylindrical microcavities," *Photonic Sensors*, 2017, 7(2): 148–156.